

# A review of the electronic structure of $\text{CaFe}_2\text{As}_2$ and $\text{FeTe}_{0.6}\text{Se}_{0.4}$

Kalobaran Maiti\*

*Department of Condensed Matter Physics and Materials Science,  
Tata Institute of Fundamental Research, Homi Bhabha Road, Colaba, Mumbai - 400 005, INDIA.*  
(Dated: March 20, 2019)

Fe-based superconductors have drawn much attention during the last decade due to the finding of superconductivity in materials containing the magnetic element, Fe, and the coexistence of superconductivity & magnetism. Extensive study of the electronic structure of these systems suggested dominant role of  $d$  states in their electronic properties, whereas the cuprate superconductors show major role of the ligand derived states. In this article, we review some of our results on the electronic structure of these fascinating systems employing high resolution photoemission spectroscopy. The combined effect of electron correlation and covalency reveal an interesting scenario in their electronic structure. The ligand  $p$  states contribution at the Fermi level is found to be much more significant than that indicated in earlier studies. Temperature evolution of the energy bands reveals signature of transition akin to Lifshitz transition in these systems.

PACS numbers: 74.70.Xa, 74.25.Jb, 71.20.-b, 79.60.-i

## INTRODUCTION

High temperature superconductivity continued to be one of the thrust area in condensed matter research for many decades, where most of the focus has been centered around the study of cuprates superconductors [1]. Discovery of superconductivity in Fe-based compounds [2, 3] renewed great attention in the study of high temperature superconductivity. Fe-based systems are significantly different from the cuprates. The parent compounds in cuprates are antiferromagnetic Mott insulators, where the insulating property arises due to strong electron correlation compared to the width of their conduction band. The antiferromagnetism gets suppressed with the charge carrier doping and superconductivity emerges beyond some critical doping. The normal phase of these materials exhibit plethora of unusual behavior such as pseudogap phase, strange metallicity etc.

On the other hand, the parent compounds of Fe-based compounds (pnictides or chalcogenides) are metals exhibiting spin density wave (SDW) phase in the ground state. Charge carrier doping in these systems leads to superconductivity via suppression of long range magnetic order in the parent compositions [4]. Interestingly, many of these Fe-based compounds exhibit pressure induced superconductivity [5, 6]. Application of pressure usually renormalizes the hopping interaction strengths due to the compression/distortion of the real lattice without significant change in the overall carrier concentration. Thus, the finding of pressure induced superconductivity expands the domain of unresolved puzzles significantly. Most interestingly, some Fe-based compounds exhibit an unusual coexistence of magnetic order and superconductivity [6, 7].

Here, we review the experimental results of two Fe-based superconductors,  $\text{Fe}(\text{TeSe})$  and  $\text{CaFe}_2\text{As}_2$  belonging to two different class of materials published ear-

lier [8–10] and try to bring out common features among these materials.  $\text{Fe}(\text{TeSe})$  group of compounds, popularly known as ‘11’ systems forms in anti-PbO-type crystal structure (space group  $P4/nmm$ ) [11], and are believed to be the most correlated ones due to their large ‘chalcogen height’ [12] (the height of the anions from the Fe-plane) [13]. The end members,  $\text{FeTe}$  exhibits spin density wave (SDW)-type antiferromagnetic transition at 65 K [14, 15] and  $\text{FeSe}$  is a superconductor below 8 K [16, 17]. Homovalent substitution of Te at Se-sites in  $\text{FeSe}$  leads to an increase in superconducting transition temperature,  $T_c$  with maximum  $T_c$  of 15 K for 60% Te-substitutions [18], despite the fact that such substitutions often introduces disorder in the system that is expected to reduce the superconducting transition temperature,  $T_c$  [19].

$\text{CaFe}_2\text{As}_2$  belong to another class of materials known as ‘122’ compounds and crystallize in the  $\text{ThCr}_2\text{Si}_2$  type tetragonal structure at room temperature, (space group  $I4/mmm$ ).  $\text{CaFe}_2\text{As}_2$  exhibits SDW transition due to the long range magnetic ordering of the Fe moments at  $T_{SDW} = 170$  K along with a structural transition to an orthorhombic phase. High pressure [5], substitution of Fe by Co, Ni [20] and other dopants induces superconductivity in  $\text{CaFe}_2\text{As}_2$ . The SDW transition is found to accompany a nesting of the Fermi surface [21, 22] along with a transition from two dimensional (2D) to three dimensional (3D) Fermi surface associated with the structural transition [23–25].

It is believed that Fe  $3d$  states play dominant role in the electronic properties of these systems in contrast to cuprates, where the doped holes possess dominant ligand  $2p$  orbital character [1]. Thus, the physics of unconventional superconductors is complex due to the significant differences among different classes of materials. Here, we show that the ligand  $p$  electrons play much more important role than what was anticipated. The temperature evolution of the electronic structure reveals interesting

scenario in these materials.

## EXPERIMENTAL

The single crystals of  $\text{CaFe}_2\text{As}_2$  were grown using Sn flux and the single crystalline sample of  $\text{FeTe}_{0.6}\text{Se}_{0.4}$  [26] was grown by self flux method. The grown crustals were characterized by  $x$ -ray diffraction, Laue, Möussbauer and tunneling electron microscopic measurements establishing stoichiometric and homogeneous composition of the sample with no trace of additional Fe in the material. The grown crystals are flat platelet like, which can be cleaved easily and the cleaved surface looked mirror shiny. Photoemission measurements were carried out using a Gammadata Scienta analyzer, R4000 WAL and monochromatic photon sources, Al  $K\alpha$  ( $h\nu = 1486.6$  eV), He I ( $h\nu = 21.2$  eV) and He II ( $h\nu = 40.8$  eV) sources. The energy resolution and angle resolution were set to 2 meV and  $0.3^\circ$  respectively for ultraviolet photoemission (UP) studies and the energy resolution was fixed to 350 meV for  $x$ -ray photoemission (XP) measurements. The sample was cleaved *in situ* (base pressure  $< 3 \times 10^{-11}$  Torr) at each temperature several times to have a clean well ordered surface for the photoemission studies. Reproducibility of the data in both cooling and heating cycle was observed. The energy band structure of  $\text{CaFe}_2\text{As}_2$  and  $\text{FeTe}_{0.5}\text{Se}_{0.5}$  was calculated using full potential linearized augmented plane wave method within the local density approximation (LDA) using Wien2k software [27]. The energy convergence was achieved using 512  $k$ -points within the first Brillouin zone.

## RESULTS AND DISCUSSIONS

As discussed above, the major difference of Fe-based superconductors with the cuprates is believed to be the character of the conduction electrons. In cuprates, the charge transfer energy (= the energy required to transfer an electron from ligand to the copper site) is smaller than the electron correlation strength [28]. Therefore, the Fermi level,  $\epsilon_F$  lies at the top of the O  $2p$  band and the electrons close to the Fermi level possess dominant O  $2p$  character. The electron correlation strength in Fe-pnictides is expected to be relatively smaller [29] and the electrons close to  $\epsilon_F$  were described to be dominated by Fe  $3d$  character. This appears to be the case in the valence band spectrum of  $\text{CaFe}_2\text{As}_2$  shown in Fig. 1(a). The  $x$ -ray photoemission (XP) spectrum at 300 K exhibits four distinct features, A, B, C and D [9]. The calculated spectral functions obtained by convoluting the band structure results with the Fermi-Dirac function and resolution broadening function exhibit good representation of the experimental spectra. It is clear that the feature A possesses dominant Fe  $3d$  contributions (dashed

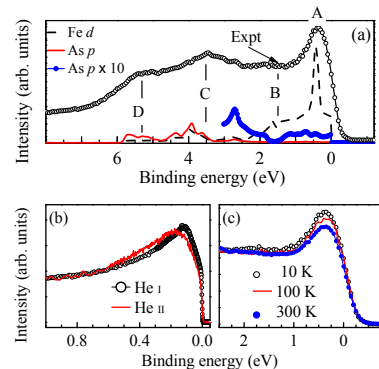


FIG. 1. (a) XP valence band spectrum of  $\text{CaFe}_2\text{As}_2$  at 300 K (symbols). Fe  $3d$  and As  $4p$  contributions obtained from ab initio calculations are shown by dashed and solid lines. The solid circles represent rescaled As  $4p$  contributions. (b) Near Fermi level feature from He I and He II excitations. (c) Evolution of the XP valence band spectra near  $\epsilon_F$  with temperatures.

line), while the As  $4p$  states (solid line) contribute at higher binding energies.

In order to learn this better, we critically investigate the electronic states close to  $\epsilon_F$ . It appears that the hybridization between As  $4p$  and Fe  $3d$  states is quite strong with significant contribution coming from As  $4p$  PDOS near  $\epsilon_F$  as shown by solid circles in the figure. This is further examined experimentally in Fig. 1(b) by comparing the spectra obtained using He I and He II excitations. The atomic photoemission cross-section for Fe  $3d$  and As  $4p$  at He I energy excitation are 4.833 & 3.856, and at He II are 8.761 & 0.2949, respectively [30]. Thus, relative intensity corresponding to As  $4p$  states will increase significantly at He I energy compared to He II energy. The comparison of the He I and He II spectra having same resolution broadening suggests that the contribution of As  $4p$  states at the Fermi level is indeed large compared to the band structure results shown in Fig. 1(a).

The temperature evolution of the feature A in the XP valence band spectra is shown in Fig. 1(c) after normalizing by the spectral intensities in the energy range beyond 1 eV binding energy. The intensity of the feature A exhibits gradual enhancement with the decrease in temperature. Valence band spectra of a correlated system exhibit signature of upper and lower Hubbard bands constituted by the correlated electronic states (often called incoherent feature) and a Kondo resonance feature called coherent feature appears at the Fermi level representing the itinerant electrons. The decrease in temperature leads to an increase in the coherent feature intensity at the cost of incoherent features [31, 32]. While such increase in spectral intensity can have other origin [33], we strongly feel, the enhancement of the feature A with the decrease in temperature shown in Fig. 1(c) can be at-

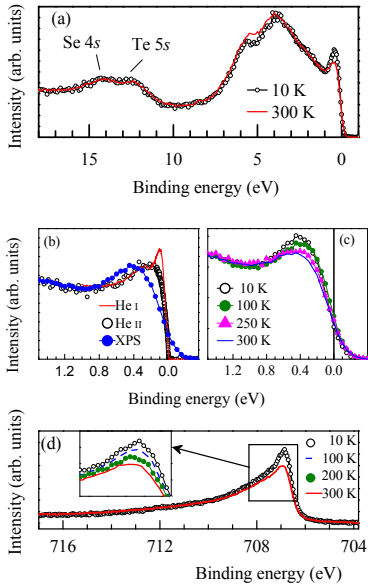


FIG. 2. (a) XP valence band spectrum of  $\text{FeTe}_{0.6}\text{Se}_{0.4}$  at 300 K (line) and 10 K (symbols). (b) Near Fermi level spectra at 10 K obtained using He I, He II and Al  $K\alpha$  lines at 10 K. (c) Temperature evolution of the near Fermi level XP feature. (d) Fe  $2p$  core level spectra. Inset shows expanded view of the well screened feature.

tributed to correlation induced effects as justified later in the text.

In Fig. 2(a), we show the valence band spectra of  $\text{FeTe}_{0.6}\text{Se}_{0.4}$  obtained using Al  $K\alpha$   $x$ -ray source at 10 K and 300 K [8]. The valence band exhibit multiple features - the feature close to  $\epsilon_F$  possess dominant Fe  $3d$  character and Te/Se  $p$  related features primarily contribute in the energy range 2 - 7 eV as also appeared in the case of  $\text{CaFe}_2\text{As}_2$ . The higher binding energy features correspond to Se/Te  $s$  states excitations. A comparison of the near Fermi level feature at 10 K obtained using different photon energies exhibit interesting scenario. The feature around 100 meV is most intense in the He I spectra indicating again large chalcogen  $p$  contributions. Decrease in temperature leads to a gradual increase in intensity of the near  $\epsilon_F$  feature as shown in Fig. 2(c) consistent with the scenario in correlated electron systems.

The correlation induced effect can be verified further by inspecting the Fe  $2p$  core level spectra shown in Fig. 2(d). The spectra exhibit an interesting evolution with temperature. The intensity of the peak around 707 eV binding energy increases gradually with the decrease in temperature (see inset). This feature is often referred as the well screened feature, where the core hole created by photoemission is screened by a conduction electron in the final state [34, 35]. Since the decrease in temperature leads to an enhancement of the coherent feature intensity with a consequent decrease in the incoherent

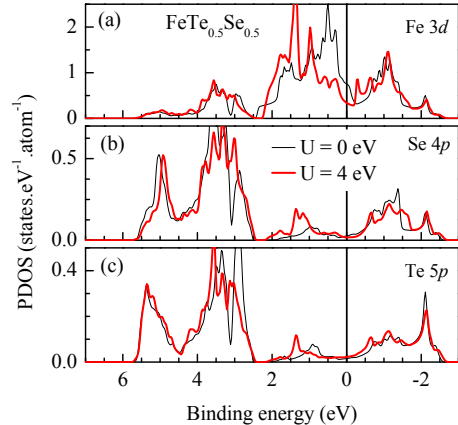


FIG. 3. Calculated (a) Fe  $3d$ , (b) Se  $4p$  and (c) Te  $5p$  partial density of states for uncorrelated (thin line for  $U = 0$  eV) and correlated system (thick line for  $U = 4.0$  eV).

feature intensity [31], the core hole is expected to be more efficiently screened at lower temperatures as more number of mobile electrons are available at low temperatures. Therefore, the temperature evolution of the core level spectra observed here can also be attributed to the correlation induced effect discussed for the valence band.

In order to investigate the dominance of  $p$  character near  $\epsilon_F$  in the experimental spectra in contrast to the prediction of the dominance of Fe  $3d$  states, we show the calculated partial density of states corresponding to the correlated and uncorrelated ground states [8]. Finite electron correlation leads to a spectral weight transfer from  $\epsilon_F$  to higher binding energies leading to an enhancement of the intensity around 2 eV (incoherent feature). Electron correlation affects the electronic states with different orbital character differently depending on their degree of itineracy in the uncorrelated system [36]. This is evident in Fig. 3 exhibiting significant transfer of the Fe  $3d$  partial density of states (PDOS) to higher binding energies. However, the Se  $4p$  / Te  $5p$  contributions increase near  $\epsilon_F$ . Thus, the relative intensity of the  $p$ -states near  $\epsilon_F$  will be enhanced significantly with respect to the Fe  $d$  states. This explains the presence of dominant  $p$  character near  $\epsilon_F$  in the experiment.

Being investigated the character of the electronic states near  $\epsilon_F$ , we now turn to the energy band structure of a typical pnictide,  $\text{CaFe}_2\text{As}_2$  - all the samples in this class of materials exhibit essentially similar electronic structure. The calculated energy bands are shown in Fig. 4(a) exhibiting  $t_{2g}$  bands close to the Fermi level, and both bonding & anti-bonding  $e_g$  bands appear away from  $\epsilon_F$ . Three energy bands having  $t_{2g}$  symmetry and de-

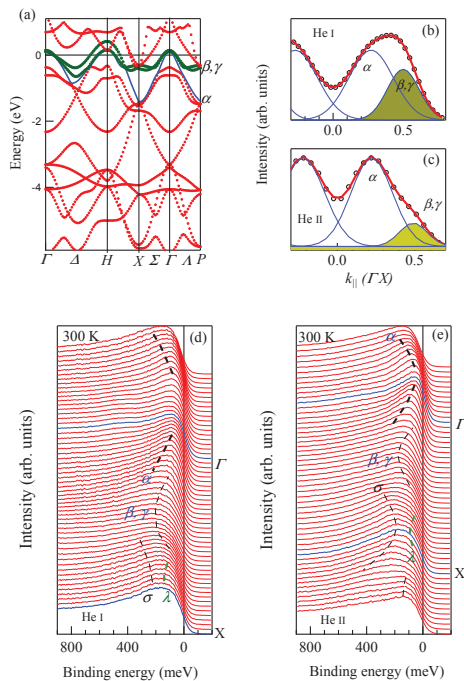


FIG. 4. (a) Calculated energy band structure of  $\text{CaFe}_2\text{As}_2$  showing three energy bands  $\alpha$ ,  $\beta$  and  $\gamma$  making three hole pockets around  $\Gamma$  point. Momentum distribution curves at 140 meV and 300 K in the (b) He I and (c) He II spectra. The lines show a typical fit exhibiting signature  $\alpha$ ,  $\beta$  and  $\gamma$  bands. Energy distribution curves as (d) He I and (e) He II photon energies and 300 K.

noted by  $\alpha$ ,  $\beta$  and  $\gamma$  in the figure cross  $\epsilon_F$  near  $\Gamma$  point forming three hole-pockets. Here,  $\Gamma$  and  $X$  points are defined as  $(0,0)$  and  $(\pi,\pi)$  in the  $xy$ -plane. The  $k_z$  values corresponding to He I and He II photon energies are ( $k_z \sim 9.5\pi/c$  and  $\sim 12.5\pi/c$ , respectively).

Various angle resolved photoemission spectroscopic measurements [23–25] show that the Fermi surface corresponding to all these three bands exhibit two-dimensional topology at room temperature, where the sample has tetragonal structure. The signature of these three bands are observed in the momentum distribution curves (MDCs) at 300 K in the He I and He II spectra shown in Figs. 2(b) and 2(c), respectively. The  $\beta$  and  $\gamma$  bands possessing  $d_{xz}, d_{yz}$  symmetry appear almost degenerate, while the  $\alpha$  band having  $d_{xy}$  symmetry distinctly appear at slightly higher binding energies [9]. The energy distribution curves (EDCs) in Figs. 2(d) and 2(e) show that all these energy bands cross,  $\epsilon_F$  in the vicinity of  $\Gamma$  point indicating presence of three hole-pockets at room temperature. An energy band  $\lambda$  is also observed forming an electron pocket around  $X$ -point. The Fermi surfaces cor-

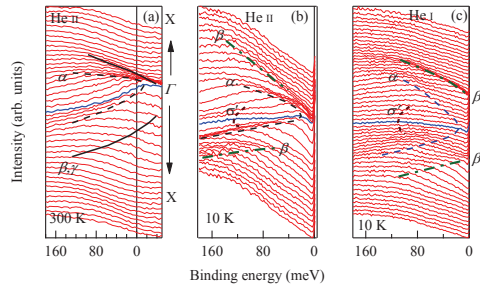


FIG. 5. Energy distribution curves (EDCs) in the He II at (a) 300 K and (b) 10 K. (c) The EDCs in the He I spectra at 10 K.

responding to  $\gamma$  and  $\lambda$  bands are nested leading to the SDW transition in these materials [21, 22].

With the decrease in temperature below the SDW transition temperature, the  $\gamma$  band hole pocket and the  $\lambda$  band electron pocket vanishes opening up a gap at the Fermi level [24, 25]. Subsequently, the crystal structure also changes from tetragonal to orthorhombic that leads to a change in the Fermi surface topology - the Fermi surface corresponding to the  $\alpha$  band exhibit  $k_z$ -dependence indicating its transition to three dimensionality [23]. It is observed that in the orthorhombic phase, the  $\alpha$ -band hole pocket is centered around  $k_z \sim 2(2n+1)\pi/c$  and it is absent around  $4n\pi/c$  in the  $k$ -plane containing  $k_z$  axis. Thus,  $\alpha$  band is expected to cross  $\epsilon_F$  at He I energy, while it will appear below  $\epsilon_F$  at He II energy. We show the He II EDCs at 300 K and 10 K in Figs. 5(a) and 5(b), respectively exhibiting exactly the same scenario. Interestingly, the  $\alpha$  band in the He I spectra also appears below  $\epsilon_F$  at 10 K as shown in Fig. 5(c) indicating the vanishing of the Fermi surface corresponding to the  $\alpha$  band at 10 K - larger intensity of the  $\alpha$  band in He II spectra compared to that in He I spectra indicate its dominant Fe  $3d$  character.

It is to note here that many of the unconventional superconductors exhibit signature of Lifshitz transition [37]. If the Fermi level is in proximity to a point separating hole- and electron-type Fermi surfaces, a small change in a tuning parameter such as doping, pressure would lead to a transition from an electron-type to hole-type Fermi surface or vice versa. This is known as Lifshitz transition. Proximity to Lifshitz transition indicates significant quantum fluctuation in the system. The signature of Lifshitz transition has been observed due to subtle change in charge carrier concentration in cuprates [37] as well as in electron doped  $\text{Ba}(\text{Fe}_{1-x}\text{Co}_x)_2\text{As}_2$  [38]. The vanishing of the hole Fermi surface corresponding to the  $\alpha$  in  $\text{CaFe}_2\text{As}_2$  as a function of temperature is interest-

ing and akin to the scenario in Lifshitz transition. These results indicate importance of Lifshitz transition in such unconventional superconductors.

## CONCLUSIONS

In summary, we presented here a review of our studies of the electronic structure of Fe-based superconductors,  $\text{FeTe}_{0.6}\text{Se}_{0.4}$  and  $\text{CaFe}_2\text{As}_2$ . A critical analysis of the experimental and band structure results indicates that the electronic states close to the Fermi level deriving the electronic properties of these materials possess significantly large  $p$  character. Thus, the difference between Fe-based and cuprate superconductors appears to be much less than what was thought earlier. The temperature evolution of the experimental spectra exhibit signature the enhancement of the coherent feature (Kondo resonance feature) at lower temperatures. The angle resolved photoemission data from  $\text{CaFe}_2\text{As}_2$  exhibit signature of Lifshitz transition as a function of temperature.

---

\* Corresponding author: kbmaiti@tifr.res.in

- [1] A. Damascelli, Z. Hussain, and Z.-X. Shen, *Rev. Mod. Phys.* **75**, 473 (2003).
- [2] Y. Kamihara *et al.*, *J. Am. Chem. Soc.* **128**, 10012 (2006).
- [3] Y. Kamihara, T. Watanabe, M. Hirano, and H. Hosono, *J. Am. Chem. Soc.* **130**, 3296-3297 (2008).
- [4] K. Ishida, Y. Nakai, and H. Hosono, *J. Phys. Soc. Jpn.* **78**, 062001 (2009).
- [5] T. Park *et al.*, *J. Phys.: Condens. Matter* **20**, 322204 (2008); H. Lee *et al.*, *Phys. Rev. B* **80**, 024519 (2009); S.-H. Baek *et al.*, *Phys. Rev. Lett.* **102**, 227601 (2009).
- [6] N. Kurita *et al.*, *Phys. Rev. B* **83**, 214513 (2011).
- [7] G. Adhikary *et al.*, *J. Phys.: Condens. Matter* **25**, 225701 (2013).
- [8] G. Adhikary *et al.*, *J. Appl. Phys.* **114**, 163906 (2013).
- [9] G. Adhikary *et al.*, *J. Appl. Phys.* **115**, 123901 (2014).
- [10] K. Maiti *et al.*, *AIP Conf. Proc.* **1512**, 15 (2013); G. Adhikary *et al.*, *AIP Conf. Proc.* **1349**, 837 (2011); G. Adhikary *et al.*, *AIP Conf. Proc.*, **1347**, 169 (2011).
- [11] M. Tegel, C. Löhner, and D. Johrendt, *Solid State Comm.* **150** 383 (2010).
- [12] K. Kuroki, H. Usui, S. Onari, R. Arita, and H. Aoki, *Phys. Rev. B* **79** 224511 (2009).
- [13] Y. Mizuguchi and Y. Takano, *J. Phys. Soc. Jpn.* **79**, 102001 (2010).
- [14] F. Ma, W. Ji, J. Hu, Z.-Y. Lu, and T. Xiang, *Phys. Rev. Lett.* **102**, 177003 (2009).
- [15] A. Subedi, L. Zhang, D. J. Singh, and M. H. Du, *Phys. Rev. B* **78** 134514 (2008).
- [16] F.-C. Hsu *et al.*, *PNAS* **105** 14262 (2008).
- [17] C.-L. Song *et al.*, *Science* **332** 1410 (2011).
- [18] C. S. Yadav, P. L. Paulose, and K. M. Subhedhar, *Euro. Phys. Lett.* **90** 27011 (2010).
- [19] A. Ghosal, M. Randeria, and N. Trivedi, *Phys. Rev. B* **65**, 014501 (2001); M. Chand *et al.*, *Phys. Rev. B* **85**, 014508 (2012).
- [20] N. Kumar *et al.*, *Phys. Rev. B* **79**, 012504 (2009); N. Kumar *et al.*, *Phys. Rev. B* **80**, 144524 (2009).
- [21] T. Kondo *et al.*, *Phys. Rev. B* **81**, 060507(R), (2010).
- [22] Q. Wang *et al.*, *arXiv:1009.0271v1*.
- [23] C. Liu *et al.*, *Phys. Rev. Letts.* **102**, 167004 (2009).
- [24] S. Thirupathaiah *et al.*, *Phys. Rev. B* **84**, 014531 (2011).
- [25] S. de Jong *et al.*, *Europhys. Letts.* **89**, 27007 (2010).
- [26] C. S. Yadav and P. L. Paulose, *New J. Phys.* **11**, 103046 (2009).
- [27] P. Blaha, K. Schwarz, G. K. H. Madsen, D. Kvasnicka, and J. Luitz, [*WIEN2k An Augmented Plane Wave + Local Orbitals Program for Calculating Crystal Properties*] [Schwarz, K. (ed.)] (Techn. Universität Wien, Austria, 2001).
- [28] K. Maiti and D.D. Sarma, *Phys. Rev. B* **65**, 174517 (2002); K. Maiti, D. D. Sarma, T. Mizokawa, and A. Fujimori, *Europhys. Lett.* **37**, 359 (1997); K. Maiti, D.D. Sarma, T. Mizokawa, and A. Fujimori, *Phys. Rev. B* **57**, 1572 (1998).
- [29] M. Aichhorn, S. Biermann, T. Miyake, A. Georges, and M. Imada, *Phys. Rev. B* **82**, 064504 (2010).
- [30] J. J. Yeh and I. Lindau, *At. Data and Nucl. Data Tables* **32**, 1 (1985); K. Maiti and D. D. Sarma, *Phys. Rev. B* **58**, 9746 (1998).
- [31] A. Georges, G. Kotliar, W. Krauth, and M. J. Rozenberg, *Rev. Mod. Phys.* **68**, 13 (1996); M. Imada, A. fujimori, and Y. Tokura, *Rev. Mod. Phys.* **70**, 1039 (1998).
- [32] S. Patil *et al.*, *J. Phys.: Condensed Matter* **22**, 255602 (2010); S. Patil *et al.* *Phys. Rev. B* **82**, 104428 (2010).
- [33] N. E. Sluchanko *et al.* *J. Exp. Theor. Phys.* **104**, 120 (2007); K. Maiti, V. R. R. Medicherla, S. Patil, R. S. Singh, *Phys. Rev. Letts.* **99**, 266401 (2007).
- [34] J. F. van Acker, *et al.* *Phys. Rev. B* **37**, 6827 (1988).
- [35] M. Takahashi and J.-I. Igarashi, *Phys. Rev B* **85**, 085128 (2012); K. Maiti, P. Mahadevan, and D. D. Sarma, *Phys. Rev. B* **59**, 12457 (1999).
- [36] R. S. Singh, V. R. R. Medicherla, K. Maiti, and E. V. Sampathkumaran, *Phys. Rev. B* **77**, 201102(R) (2008); K. Maiti, *Solid State Commun.* **149**, 1351 (2009).
- [37] K. -S. Chen, Z. Y. Meng, T. Pruschke, J. Moreno, and M. Jarrell, *Phys. Rev. B* **86**, 165136 (2012).
- [38] C. Liu, *et al.* *Nat. Phys.* **6**, 419 (2010).